Poly(L-lysine) and Clay Nanocomposite with Desired Matrix Secondary Structure: Effects of Polypeptide Molecular Weight

ROHAN A. HULE, DARRIN J. POCHAN

Department of Materials Science and Engineering and Delaware Biotechnology Institute, University of Delaware, Newark, Delaware 19716

Received 19 June 2006; revised 15 September 2006; accepted 22 September 2006
DOI: 10.1002/polb.21027
Published online in Wiley InterScience (www.interscience.wiley.com).

ABSTRACT: Nanocomposites (NC) were formed using cationic poly(L-lysine) (PLL), a semicrystalline polypeptide, that was reinforced by sodium montmorillonite (MMT) clay via solution intercalation technique. By varying solution conditions such as pH, temperature, and polypeptide concentration in the presence of clay platelets, the secondary structure of PLL was controllably altered into α-helical, β-sheet, and random coil. The high molecular weight polypeptide shows a strong propensity to fold into the β-sheet structure when cast as films, irrespective of the initial secondary structure in solution. Nanocomposite local morphology confirms intercalated MMT platelets with PLL over a wide range of compositions. ©2006 Wiley Periodicals, Inc. J Polym Sci Part B: Polym Phys 45: 239–252, 2007

Keywords: biomaterials; clay; nanocomposites; polypeptides; secondary structure; α-sheet; β-helix

INTRODUCTION

The formation of nanocomposites from natural, synthetic, and functionalized inorganic fillers has bloomed into a robust science. A rational way to distinguish these composites is based on the physical dimensions of the filler; a composite having a reinforcing agent with at least one dimension in the nanometer range is consequently called a nanocomposite. One widely investigated and promising class of nanocomposites has been polymer layered clay silicates. Clay silicates are composed of a regular stacking of silicate layers bound together by weak interatomic forces.[1,2] Clay nanocomposites exhibit impressive enhancement of various physical properties because of the effective interaction of the clay with the matrix polymer across the large surface area available for polymer adsorption and stability of the clay platelets. Better mechanical[3] and barrier properties,[4] flame retardant behavior[5] with self-extinguishing characteristics,[1] and optical transparency[1] are some of the advantages offered by this class of nanocomposites. The properties of the matrix, the filler, and processing conditions dictate the final exclusive or coexistent morphology, including microphase separated clay tactoids in the polymer matrix, an intercalated nanocomposite, and/or an exfoliated nanocomposite.[3] We have used sodium montmorillonite (MMT) as the inorganic filler for this study. MMT is hydrophilic in nature and belongs to the 2:1 layered phyllosilicate group that forms stable dispersions in water. Once uniformly dispersed in solution, it has negatively charged layers that are counterbalanced by cations (Na^+, in this case),[2] enabling electrostatic interaction of the filler and the polymer matrix. These cations are always present unless they have been stripped by some caustic process.[6,7]

This article contains supplementary material available via the Internet at http://www.interscience.wiley.com/jpages/0887–6266/suppmat

Correspondence to: D. J. Pochan (E-mail: pochan@udel.edu)

Journal of Polymer Science: Part B: Polymer Physics, Vol. 45, 239–252 (2007)

The use of biocompatible and/or biodegradable polymers in these nanocomposites[4,8–10] is driven by environmental concerns, reusability, and a multitude of applications. Polymers that are biodegradable *in vivo* open a wide range of applications in biomedical areas such as tissue engineering, drug-delivery,[11] biotemplate for the synthesis of inorganic materials,[12–17] and composites for bone and tissue regeneration[18] to name a few. Polymer layered silicate nanocomposites have also been designed from biocompatible polymers.[19] Polypeptides as matrices provide a further array of opportunities in materials design and application in terms of a unique ability to adopt specific secondary, tertiary, and quaternary structures, a feature not available with synthetic polymers.[20] Functionality can also be incorporated by the use of natural and non-natural amino acids with desired activity at specific sites along the polypeptide backbone. The unique blend of desired secondary structure and precise chemical and biological functionality offered by this class of molecules inspired us to incorporate them into nanocomposites. Thus, understanding the effect of secondary structure of these polypeptides on the morphological control they exhibit in nanocomposites is vital to the future building of advanced materials with requisite design and function.

The polypeptide used in this study is poly(L-lysine).HBr (PLL), a homopolymer that is cationic at neutral pH. Prior work[21] has produced nanocomposites from PLL ($M_n = 2.7 \times 10^5$ g/mol, PDI = 1.28) and MMT that exhibited enhanced storage moduli and thermal properties comparable to other widely explored biomaterials[22] and engineering thermoplastics.[23] Herein, the potential applicability of these materials is further investigated by studying the effect of the secondary structure of the polypeptide matrix on the properties of the final nanocomposite. PLL is a good choice for such a study, as it can display a variety of secondary structures: the random coil, α-helix, and β-sheet, in aqueous solution.[24] Moreover, transition from one conformation to the other can be easily achieved using pH,[25] temperature,[26] salt concentration,[27] or alcohol content[28] as an environmental stimulus. One of the most definitive studies on the effect these solution stimuli have on the secondary structure of PLL was done by Greenfield and Fasman. They calculated the percentage of the different secondary structures that existed at various solution conditions using optical rotatory dispersion[29] and circular dichroism (CD).[25] In addition, the secondary structure of PLL in solution (H_2O and D_2O) and in solid state has been extensively studied using infrared spectroscopy.[30] The effect of various salts on the secondary structure of PLL has been studied by Raman spectroscopy.[31] The thermodynamics of these transitions have also been accurately mapped using potentiometric titrations.[32] A wealth of information pertaining to the effect of chain length on the secondary conformational transitions is also available. Jackson et al.[33] observed that the transition from α-helix to β-sheet occurs at a minimum chain length. Studies on single crystals of PLL and incorporation of these ideas to template nanostructure have also been very helpful in this investigation.[34] This significant past work to understand the mechanism of secondary structure transitions in PLL is a critical foundation upon which this current nanocomposite effort is based.

Another motivating factor for this study is the reduction in entropy caused by a change from the random state to a specific secondary structure observed in polypeptides. The lower entropy of a polypeptide in an α-helical or a β-sheet structure when compared with its random form eases its adsorption onto a flat, solid surface (*e.g.*, clay). Previous efforts[35,36] have shown that an increase in the helical fraction of a polypeptide, amounting to greater chain stiffness, decreases the critical adsorption energy. Given that the secondary structure of PLL can be controlled, a change in adsorption, and hence final nanocomposite properties, can be expected.

Herein we report the synthesis of nanocomposites from PLL and MMT via the solution intercalation method and the effect of secondary structure of the polypeptide on the final nanocomposite. The secondary structure of PLL and the changes accompanying clay addition in aqueous solution have been studied by CD spectroscopy. Fourier transform infrared (FTIR) spectroscopy was also used to study the secondary structure of pure PLL and of PLL-MMT solutions prior to casting films. FTIR was performed on final PLL-MMT nanocomposite films as well. X-ray diffraction (XRD) and transmission electron microscopy (TEM) were employed to investigate nanocomposite formation and local morphology.

EXPERIMENTAL

Materials

Poly(L-lysine).HBr (PLL) with varying molecular weights of 84,000, 25,500, and 9200 g/mol were

purchased from Sigma–Aldrich and used without further purification. The clay, Wyoming Na^+-Montmorillonite (Swy-2) (MMT) with a cation exchange capacity of 76.4 meq/100 g, was obtained from the Clay Mineral Repository at University of Missouri. The buffers used in this study were potassium phosphate (KH_2PO_4) with a molecular weight of 136.09 g/mol (pH 7 and 11.6) and bis–tris propane (BTP) (pH 11.6) with a molecular weight of 282.3 g/mol. Both were obtained from ICN Biomedicals.

MMT Purification

MMT (15 g) was gradually added to a large excess of deionized (DI) water and stirred overnight. The solution was kept undisturbed for a day to allow for sedimentation of the impurities. The decanted solution was similarly treated twice to separate the impurities completely. The purified clay solution was then centrifuged to obtain clay, which was further dried at 100 °C for 48 h to remove final traces of water. The MMT clay was then ground to a homogeneous powder using a mortar and pestle.

Buffer Preparation

Concentrations of 1, 50, and 100 mM buffer used for various characterization techniques were prepared by adding the appropriate amounts of the buffer to milliQ water and the pH adjusted by sodium hydroxide. Phosphate was used at pH 7 and pH 11.6, while BTP was used at pH 11.6.

Nanocomposite Preparation

All nanocomposites were prepared using the solution-intercalation film-casting technique. Six different compositions with increasing clay contents from 2, 5, 10, 15, 20, and 25 wt % were investigated. 120 mg of PLL (MW = 84,000 g/mol) was used in each of these compositions. The pH 7 buffer media resulted in a random coil conformation, while the pH 11.6 buffer was used for an α-helical conformation. A measured amount of the clay was suspended in 8 mL of the appropriate buffer and sonicated for 15 min with 5 min intervals using a Misonix 300 Sonicator to ensure a homogeneous suspension of the clay. PLL was then added to this suspension and the solution was stirred on a vortexer to enhance dissolution. This solution was cast in poly(fluoro acetate) (PFA) petri dishes. Evaporation was carried out in a hood to ensure controlled environment with an aluminum foil tent covering the dishes to avoid unwanted air drafts that disrupt evaporation rates. Films formed after 3 days were carefully peeled out with tweezers; use of PFA made film removal easy.

Characterization

Circular Dichroism Spectroscopy

Circular dichroism (CD) measurements on PLL were carried out on a Jasco J-810 spectropolarimeter. 1 mg/mL (11.9 μM) solution of the polypeptide prepared in the appropriate buffer was diluted with buffer solutions to remain within the measurable range of the CD instrument. 30 μL of the stock polypeptide solutions was mixed with 270 μL of the respective buffer solutions in a 1 mm pathlength quartz cell. The cell was inverted several times to achieve uniform concentration throughout. Thus, the final concentration of the polypeptide after dilution with 50 mM phosphate buffer was 1.19 μM. Similarly, 1 mM BTP was used to dilute the polypeptide stock solution prepared in BTP. A different concentration of BTP was used for dilution as the concentration originally used (50 mM) led to a very high dynode voltage (above 800 V) and hence unreliable CD signals. The cells were placed in the instrument holders pre-equilibrated at 25 °C, immediately after sample preparation. Wavelength scans were performed from 260 to 190 nm for every 5 °C until 70 °C. The samples were equilibrated at each temperature for 10 min before recording the spectra in each cell. During kinetic studies, the temperature was kept constant for varying amounts of time and the CD spectra were measured at the beginning and the end of the time period at a particular temperature. To study the effect of the addition of MMT on PLL, two different concentrations of the polypeptide were used: 1.19 and 0.595 μM of PLL. A 1 mg/mL solution of MMT in DI water sonicated for 15 min was prepared separately. Increasing amounts of the clay solution, starting from 5 to 50 μL, were added to the PLL solution in the CD cell. The cell was then diluted with 1 mg/mL BTP buffer at an appropriate pH to make up the volume to 500 μL. All clay studies using CD were done at room temperature. The pH was found to remain constant with increasing clay content. The rest of the experimental procedure pertaining to data collec-

tion remained same. Mean residue ellipticity (MRE) [θ] was calculated from the equation [θ] = (θ_{obs}/10lc)/r, where θ_{obs} is the measured ellipticity in millidegrees, l is the length of the cell in centimeters, c is the molar concentration, and r is the number of residues.

Infrared Spectroscopy

Solution infrared spectra were collected on a Thermo Nicolet Nexus 870 E.S.P. spectrometer using a zinc selenide flow cell and Omnic v6.0 software for data analysis. Resolution and number of scans were kept constant at 4 cm^{-1} and 256, respectively. The samples for studying the interaction of clay with PLL were prepared in 50 mM BTP, pH 11.6 in D_2O to obtain a concentration of 1 mg/mL. The solution was inserted in the flow cell using a syringe, taking care that no air bubbles were formed, and the spectra were recorded. To study the interaction of clay with PLL, a spectrum of 1 mg/mL PLL in the aforementioned buffer was recorded. One milligram of MMT was added to this solution and sonicated for 15 min to ensure uniform dispersion. The clay was then centrifuged at a speed to 14,000 rpm on an Eppendorf centrifuge for 15 min to settle out all the clay present. The supernatant was fed in the flow cell again using a syringe and the spectrum recorded. A control with no clay was subjected to similar treatment.

The secondary structure of PLL in solution under conditions identical to those prior to casting films was also studied using FTIR. For these experiments, a concentration of 15 mg/mL PLL was used, the same concentration that is used for casting nanocomposite films. All solution experiments were carried out in D_2O using 50 mM BTP buffer at pH 11.9. A low molecular weight of PLL solution (MW = 25,500 g/mol) and 2, 5, and 10 wt % MMT-PLL solutions (MW = 84,000 g/mol) were also studied under similar concentration and pH conditions. These experiments were carried out in the zinc selenide flow cell as described earlier.

Infrared spectra of all PLL-MMT nanocomposite films were recorded on Bruker Tensor 27 spectrometer in the ATR mode and data analysis was performed using OPUS v5.0 software. A section of the nanocomposite film having uniform thickness and texture was placed on the diamond surface and was pressed firmly using a fixture to ensure that the film was in contact with the diamond crystal. A similar arrangement without the film gave a background spectrum that was subsequently subtracted from the sample absorbance spectrum. All film spectra were recorded in this fashion. For the analysis in Figure 6, the ratio of intensities at 1620 cm^{-1} (β-sheet peak) and 1650 cm^{-1} (α-helix peak) was taken. This ratio was calculated for each of the clay loading. Four readings were taken at each clay concentration and the average plotted.

X-ray Diffraction

X-ray diffraction (XRD) patterns of the nanocomposite films were collected at the National Synchrotron Light Source, Brookhaven National Laboratory, beamline X10A. All the films were attached to the aluminum sample holder with a circular cutout using scotch tape. The samples were exposed to the beam for 30 s and the scattering patterns were recorded on a Bruker 2D CCD camera. Monochromatic synchrotron X-ray radiation (λ = 1.54 Å) was used in all data collection. The sample to detector distance was calibrated using silver behenate as a standard. The data was analyzed using Bruker SAXS v3.324 software. XRD experiments on neat MMT clay were performed using an Anton Paar SAXSess. The diffraction pattern was collected on phosphor image plates that were subsequently optically scanned to convert to an intensity plot. The 1D plot of intensity *versus* 2θ was obtained by integrating this intensity plot along the central area. Data analysis was done by SAXS Quant v1.01.1804. In order for the MMT peak to be seen unambiguously, background (scotch tape) subtraction was performed.

Transmission Electron Microscopy

TEM bright field imaging was performed on a JOEL 2000FX microscope with an accelerating voltage of 200 kV. Film samples were microtomed into ultra thin slices <80 nm using a diamond knife to preserve the *in situ* structure of the nanocomposites. Since the glass transition temperature (T_g) of PLL is around 56 °C, it was possible to microtome at room temperature. The microtomed films were collected with single hair brushes on carbon-coated copper grids. Images were recorded on Kodak negative films.

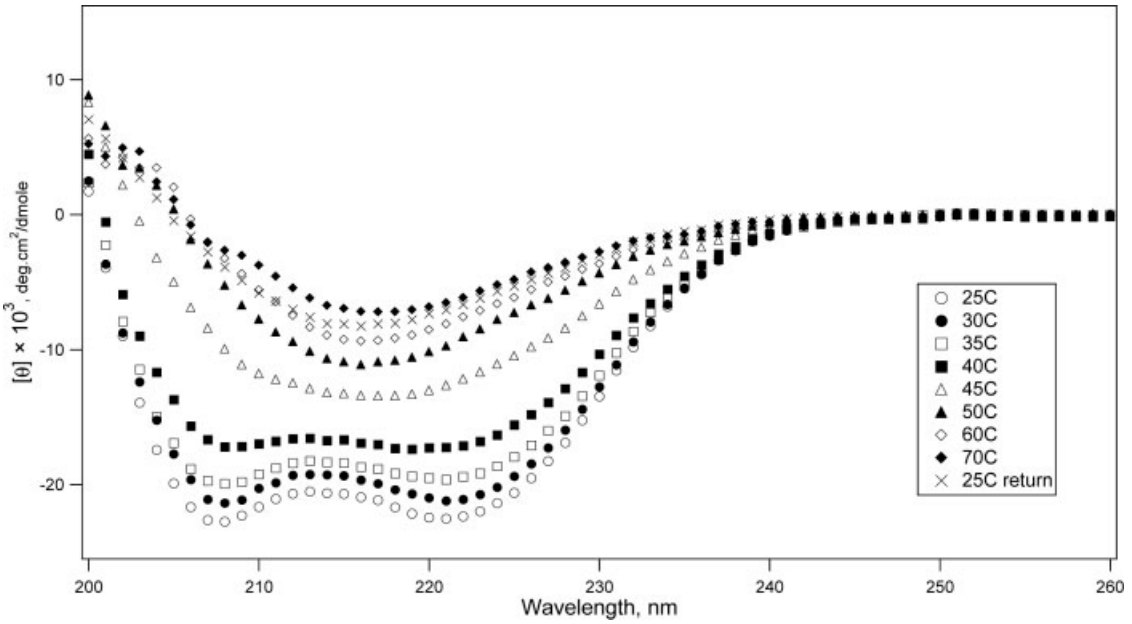

Figure 1. CD spectra of 0.09 mg/mL PLL in 1 mM BTP at pH 11.6. Wavelength scans are performed from 200 to 260 nm at varying temperatures from 25 to 70 °C. The scans show a clear secondary structure transition in PLL from an α-helical structure to a β-sheet above 45 °C. This structure remains stable even on return to 25 °C.

RESULTS

Conformational Characterization in Aqueous Solutions

The knowledge of dilute solution properties of PLL and the effect of MMT addition to PLL in solution is crucial to the design of nanocomposites with the desired secondary structure. CD was used to characterize the secondary structure of PLL in aqueous solution. pH and temperature were used as the stimuli to produce the secondary structural transition. This was followed by a study of the effect of the addition of MMT to aqueous PLL solutions. Figure 1 shows a plot of $[\theta]$ versus wavelength for 0.09 mg/mL PLL dissolved in 1 mM BTP at pH 11.6. Since CD spectra cannot be obtained for high concentrations of PLL, a low concentration of the polypeptide and buffer was chosen. The data show a minimum in intensity at 222 and 208 nm, a feature that is known to be indicative of an α-helical conformation.[25] With increasing temperature, the minimum shifts to approximately 216 nm, which is known to be a β-sheet conformation[24] and decreases in intensity. There is no change in the position of the minimum after 45 °C and even after return from 70 to 25 °C. It is known from earlier studies that PLL forms an α-helix at pH $\geq$ 10.5. The lysine side chain is almost completely deprotonated at such high pH (pK_a of lysine is ~10.54). As the temperature is raised slowly, a β-sheet structure is obtained above 45 °C and remains even as the temperature is increased to 70 °C and then decreased back to 25 °C. This confirms that the transition from α-helix to the β-sheet form of PLL is irreversible at temperatures above 45 °C. We have found that β-sheet remains stable for periods at least as long as a week. Similar wavelength scans on low molecular weight PLL (see supplemental information, Fig. S1) reveal no change in the secondary structure as the temperature is increased from 25 to 70 °C. Another interesting observation was the kinetic dependence of this transition on temperature. It takes approximately 30 min for the complete helix to sheet transition at 45 °C as opposed to less than a minute at 65 °C. The high temperature promotes the jump over the activation barrier to form β-sheet, essentially an interchain hydrogen bonding event.

Further, we studied the effect of the addition of MMT on the secondary structure of PLL. A 1 mg/mL solution of clay in 1 mM BTP, pH 11.6, sonicated for 10 min was added to the same concentration of PLL (1.19 μM). In this experiment, the concentration of PLL was kept constant

while the clay concentration was increased from 0 to 0.01 wt %. The clay percentages in these solution studies are with respect to the total volume of the solution. Similar procedures were repeated at a lower concentration of PLL (0.595 μM) (data not shown) and at different pH (pH = 7). The data for pH 11.6 and pH 7 are shown in Figure 2(A,B), respectively. As shown, the [θ] values decrease as MMT is added to the polypeptide solution. A similar decrease in the [θ] occurs at pH 7; solution conditions at which the spectra show a minimum at 198 nm [Fig. 2(B)]. A minimum at 198 nm corresponds well with earlier studies that indicate a random coil conformation.[25] At pH 7, the lysine side chains are charged and consequently repel each other, resulting in a random conformation. A decrease in the [θ] values is due to the interaction between the PLL chains and MMT platelets that reduced the PLL available in the solution.

To confirm the interaction between MMT and PLL chains in solution, FTIR spectroscopy was performed on solutions of PLL at 1.19 μM taken in D_2O. D_2O was used since its absorbance peak does not interfere with the primary amide region of PLL. Next, a 1 mg/mL solution of clay was added to the peptide solution. The combined solution was subsequently centrifuged at 14,000 rpm for 15 min to remove all traces of clay. The absorbance of the supernatant (PLL in D_2O after clay addition) was measured again. The corresponding data are shown in Figure 2(C). As is clearly seen in this figure, the absorbance of PLL decreases after the addition of the clay. Consequently, we conclude that PLL specifically interacted with the clay and, after adsorption onto clay platelets, was removed from the solution during centrifugation. This decrease in PLL concentration led to a change in the magnitude of absorbance. With the knowledge that PLL interacts with clay, we can now analyze the CD data presented in Figure 2(A,B). As the clay concentration is increased, higher amounts of PLL interacts with the clay, which decreases the PLL concentration in solution translating to a decrease in the [θ] values. The same phenomenon occurs at pH 7 and at lower PLL concentrations (data not shown). At pH 7, the lysine side chains are positively charged and interact favorably with the negatively charged clay layers. As the pH is increased, some of the PLL side chains are deprotonated and the polypeptide assumes a helical conformation. However, there are residual charges on the surface of the helix that enable positive interaction between the helix and clay surface. Besides this, studies[35,36] show a decrease in the critical adsorption energy with an increase in the helical fraction of a polypeptide. This decrease in the adsorption energy at high pH values eases PLL adsorption onto MMT surface. These results prove that the clay platelets interact favorably with PLL and addition of MMT does not lead to a change in the secondary structure of the polypeptide at the concentrations investigated. Thus, they provide an insight into the clay–polymer interactions that go on during the initial steps of solution-intercalation film-casting technique used for nanocomposite formation.

Conformational Characterization in Solution and Films

FTIR was performed to determine the secondary structure of the polypeptide prior to casting and in films in addition to investigate the effect of clay addition on the secondary structure of PLL in final film form. Spectra run on buffered PLL solutions in D_2O with concentration and pH conditions identical to ones used for the casting process are shown in Figure 3 with a maximum at 1640 cm^{-1}. These spectra include high (MW = 84,000 g/mol) and low (MW = 25,500 g/mol) molecular weight PLL solutions as well as a 2 wt % MMT-PLL (MW = 84,000 g/mol) solution with PLL concentrations of 15 mg/mL. Increasing the MMT content to 10 wt % did not change the position of this maximum (data not shown). Spectra of MMT in the buffer do not show any

Figure 2. (A) CD spectra of PLL with increasing MMT addition from 0 wt % (○), 0.008 wt % (□), and 0.01 wt % (△) at 0.119 μM PLL, pH 11.6, 1 mM BTP, room temperature. Minima at 222 and 208 nm indicate α-helical structure. There is a decrease in the [θ] as clay concentration is increased. (B) CD wavelength spectra of 0.119 μM PLL in 1 mM pH 7 BTP buffer. Clay concentration is increased through 0 wt % (○), 0.005 wt % (□) to 0.01 wt % (△). A minimum is seen at 198 nm, indicating random coil structure. [θ] values steadily decrease with increasing MMT concentration. (C) FTIR absorbance of PLL shown here as a function of wavenumber before (○) and after (□) MMT addition. Note that both spectra are of PLL alone without any clay in the solution. A decrease in the absorbance after the clay reacted with PLL and was centrifuged out indicates interaction of PLL with MMT.

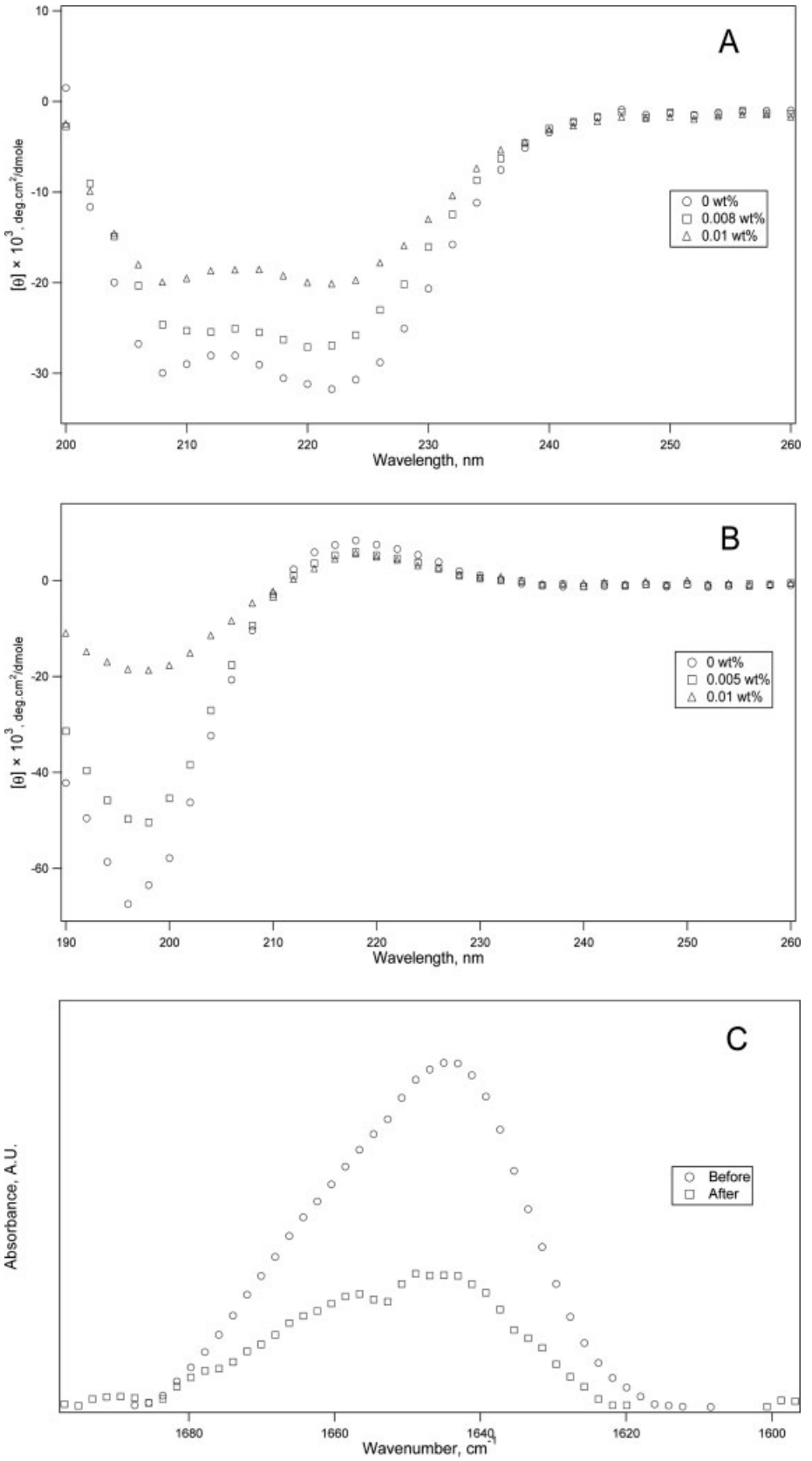
A
[θ] × 10^3, deg.cm^2/dmole
Wavelength, nm
0 wt%
0.008 wt%
0.01 wt%
B
[θ] × 10^3, deg.cm^2/dmole
Wavelength, nm
0 wt%
0.005 wt%
0.01 wt%
C
Absorbance, A.U.
Wavenumber, cm^-1
Before
After

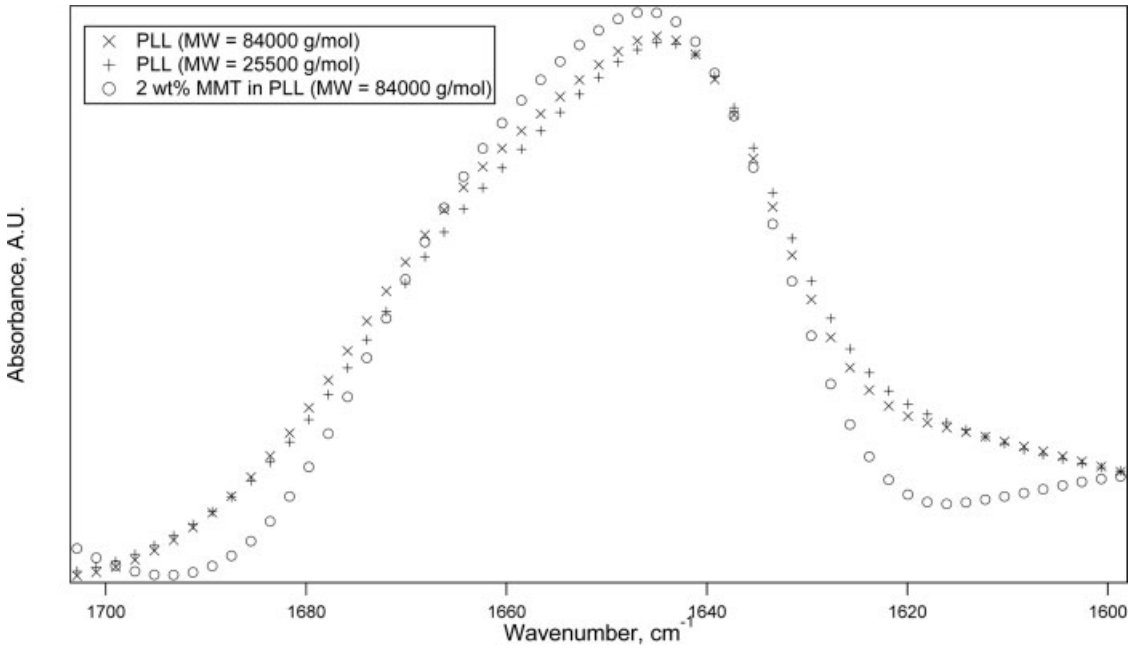

Figure 3. Solution FTIR spectrum of 15 mg/mL PLL of varying molecular weights in 50 mM BTP prepared in D_2O at pH 10.4. A low (+) and high (×) molecular weight PLL as well as 2 wt % MMT-PLL solution (○) was used for these experiments. All spectra show a peak at 1640 cm^{-1}, corresponding well with an α-helical structure.

features in this region (1600–1700 cm^{-1}). Studies involving infrared spectroscopy of PLL in D_2O have indicated that this peak results from an α-helical structure.[33] There is a 10 cm^{-1} shift in the peak position due to change in the peptide state from film to D_2O solution.[33]

Films were cast as described in the experimental section. A 50 mM BTP buffer at pH 11.6 used in all solutions resulted in an α-helical conformation. A concentration of 15 mg/mL of PLL was used in all solutions used to cast the nanocomposite films; clay content was varied from 2 to 25 wt %. The spectra for the neat PLL film and different nanocomposite samples with varying clay content are shown in Figure 4. All spectra were collected in ATR mode as described earlier in the experimental section. As seen, all spectra, irrespective of the clay content, show maxima in absorbance intensity at 1620 and 1650 cm^{-1} and a smaller peak at 1690 cm^{-1} in the amide-I region. The intensity of these peaks is directly related to the thickness of the film. Since it is not possible to completely control film thickness during casting causing variation with each sample, intensities are compared within a particular spectrum and not among spectra of different clay loadings. Spectra showing peaks at 1620 and 1690 cm^{-1} correspond well with those reported for β-sheet poly(L-lysine).[30] The peak at 1690 cm^{-1} is normally attributed to antiparallel β-sheet, commonly found in synthetically prepared polypeptides. The peak at 1650 cm^{-1} can be ascribed to α-helical PLL structures.[31] Moreover, a comparison of the intensities at 1620 and 1650 cm^{-1} indicates a higher amount of β-sheet structure when compared with α-helix, assuming that the absorbance intensity is indicative of the relative amount of secondary structure. Hence, it can be concluded from the spectra that PLL adopts β-sheet as the major secondary structure and α-helix as the minor one in films. Nanocomposite films (2 wt % MMT) cast from low-molecular-weight PLL (Fig. 5) reveal a secondary structure richer in an α-helical structure *versus* β-sheet relative to conformations observed in high molecular weight films. Experiments with PLL of even lower molecular weight (MW = 9200 g/mol) failed to form contiguous films and hence could not be tested.

The above discussion indicates that PLL adopts an α-helical structure in the solution, while a β-sheet structure is the major one in cast films. The β-sheet forming tendency is found to be strongly dependant on molecular weight as well. It has been found that high

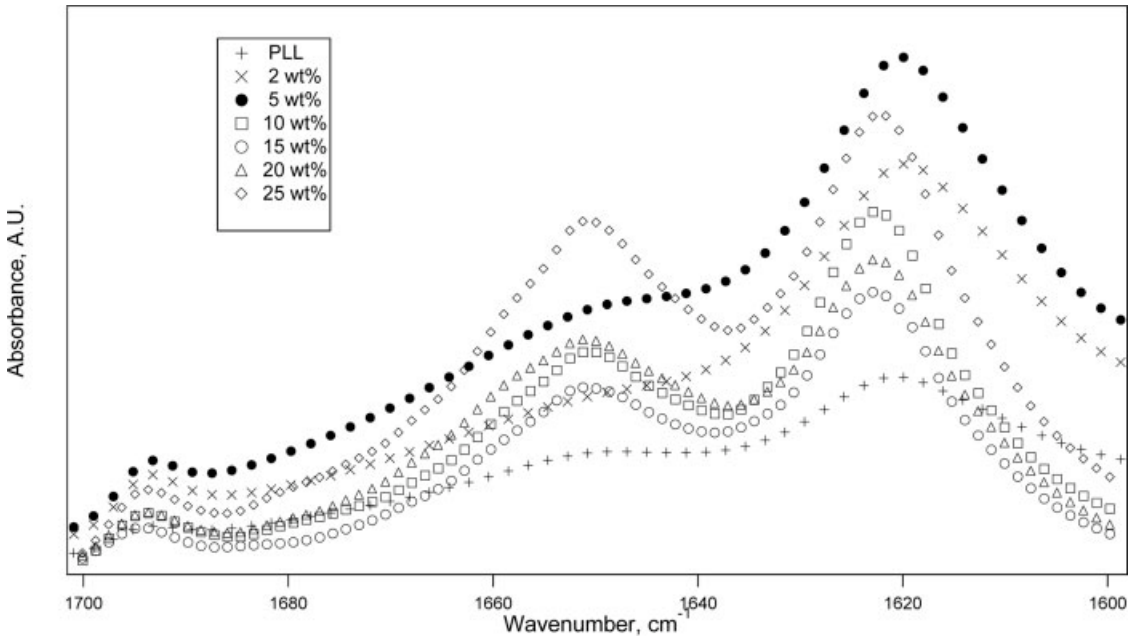

Figure 4. FTIR spectra of PLL-MMT nanocomposites with increasing clay loading from 0 wt % (+), 2 wt % (×), 5 wt % (●), 10 wt % (□), 15 wt % (○), 20 wt % (△), and 25 wt % (◇). All samples were films cast from aq. solutions containing 120 mg PLL in 8 mL 50 mM BTP buffer at pH 11.6. The peak at 1620 cm^{-1} and the shoulder at 1695 cm^{-1} correspond to β-sheet structure and an antiparallel arrangement, respectively. The peak at 1650 cm^{-1} represents the α-helical structure. The higher absorbance intensity at 1620 cm^{-1} when compared with 1650 cm^{-1} indicate β-sheet as the major component.

molecular weight PLL has a propensity to form β-sheet when compared with α-helical films formed from lower molecular weights.[33] Since high-molecular-weight PLL (84,000/575 residues) was used, it tends to fold into a β-sheet during the film formation process. Next, we compare the change in secondary conformation with the addition of clay (Fig. 6) in terms of the ratio of peak intensities at 1620 and 1650 cm^{-1} (β-sheet/α-helix) for different clay loadings in the nanocomposite. There is a slight decrease in the ratio of β-sheet/α-helix with the clay percentage (within the margin of error in these measurements), leading to the conclusion that there is a slight increase in the α-helical content with increasing clay content, although β-sheet still dominates.

X-ray Diffraction

XRD patterns of neat MMT, neat PLL film, and the PLL-MMT nanocomposites having 10, 15, and 20 wt % clay were obtained as explained in the experimental section (Fig. 7). The diffraction pattern for neat PLL shows two peaks characteristic of the semicrystalline nature of PLL. Further, the basal d-spacing of the pristine MMT clay layers can be seen as a peak at $2\theta = 8^{\circ}$, corresponding to $d = 10.84$ Å. This represents the spacing between the silica layers that constitute the clay structure. All nanocomposite diffraction patterns have a peak at 18.12 Å, corresponding to the MMT clay intercalated with PLL that increases the gallery spacing from ~10 Å. The peak at 18 Å is quite broad, implying a broad distribution of the interlayer spacing. A peak assignment for a neat PLL film cast from a pH 11.6 buffer has been done to further elucidate the origin of diffraction peaks from the PLL film (see supplemental information, Fig. S2). It may be pointed out that PLL exhibits a β-sheet structure as the major component in film form.

Investigations on the formation and morphology of PLL single crystals have shown the distance between two PLL α-helical chains separated by a counterion to be ~18 Å.[37,38] If such an α-helical chain was intercalated between clay layers, the effective interlayer spacing would have to be a minimum of 28 Å. Since all the dif-

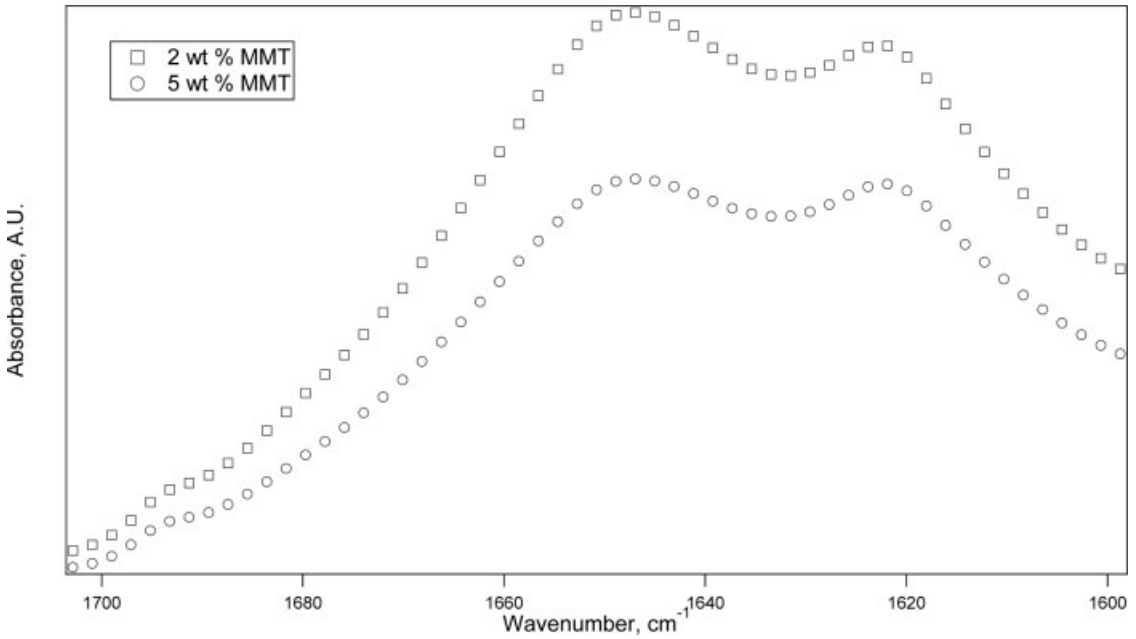

Figure 5. FTIR spectra of 2 and 5 wt % MMT in PLL (MW = 25,500 g/mol) films cast from aq. solution containing 120 mg of PLL in 8 mL 50 mM BTP buffer at pH 11.9. The peak at 1620 cm^{-1} and the shoulder at 1695 cm^{-1} correspond to β-sheet structure and an antiparallel arrangement, respectively. The peak at 1650 cm^{-1} represents the α-helical structure.

fraction data presented here has an interlayer spacing of ~18 Å, it is reasonable to believe that the intercalating polymer chain in all nanocomposites is either in random coil or β-sheet form. An interesting future subject of research using quantitative XRD could be the possible change

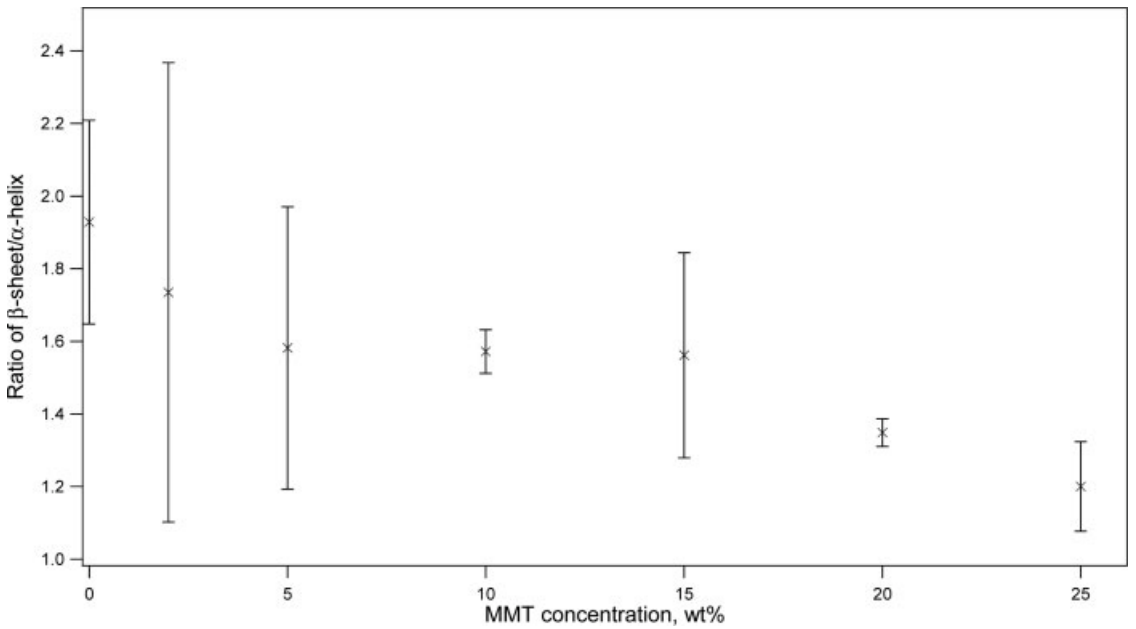

Figure 6. Ratio of peak intensity at 1620 cm^{-1} to 1650 cm^{-1} for different clay loadings for the spectra shown in Figure 4. The peaks at 1620 and 1650 cm^{-1} are attributed to β-sheet and α-helix PLL respectively.

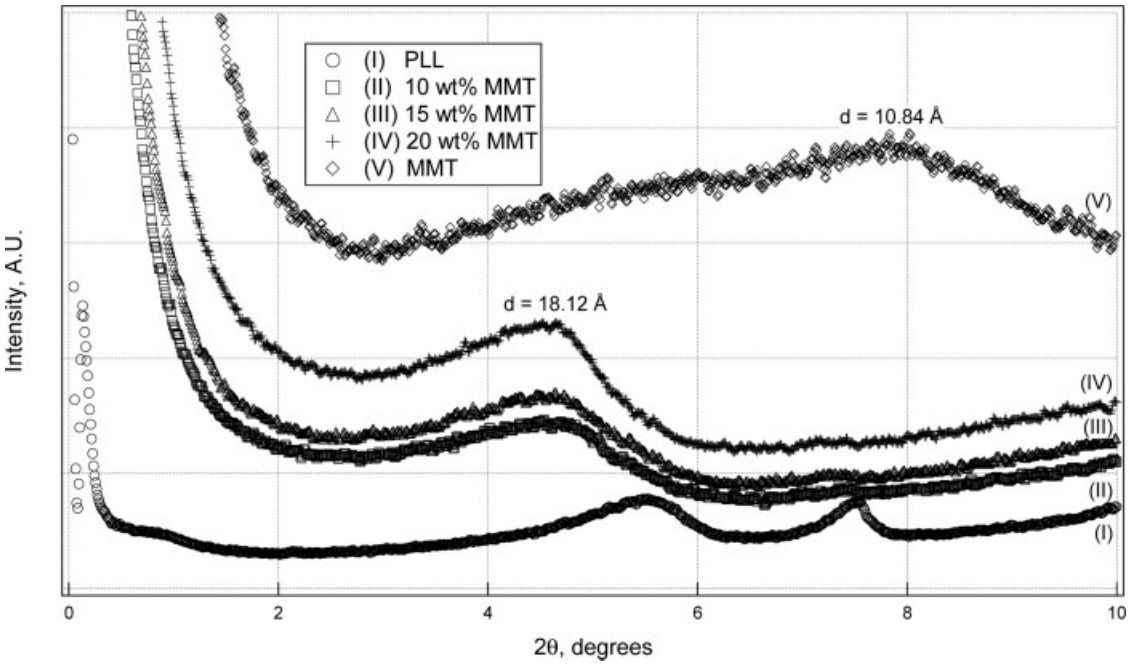

Figure 7. XRD patterns of neat PLL (○), nanocomposites with 10 wt % (□), 15 wt % (△), and 20 wt % (+) clay loading and pristine MMT (◇). The two peaks seen in the neat PLL diffraction pattern represent the primary crystal diffraction peaks. The first order reflection originating from pristine MMT interlayer spacing is at 10.84 Å. The intercalation by PLL chains lead to an increase in this spacing to 18.12 Å. This peak is seen in all nanocomposite samples irrespective of the clay loading.

in the absolute content of the crystal phase due to clay addition or processing of the nanocomposites.

Transmission Electron Microscopy

A typical TEM micrograph of the 2 wt % nanocomposite is shown in Figure 8(A) and clearly shows intercalated clay layers. Similar observations can be made in Figure 8(B–D), micrographs of nanocomposite films with 5, 10, and 15 wt % clay loading, respectively. Intercalated clay layers can also be observed in Figure 8(E), a 2 wt % clay in low (MW = 25,500 g/mol) molecular weight PLL nanocomposite film micrograph. The dark regions are clay tactoids normal to the electron beam, thus making it difficult to determine whether they are intercalated or exfoliated. Other nanocomposite samples with higher clay loadings give similar results (data not shown). The spacing between clay layers in the intercalated regions gives rise to XRD peaks. The measured interlayer spacing from TEM is consistent with XRD data. This data stresses the favorable interaction between PLL and clay, resulting in good nanometer range dispersion.

DISCUSSION

The first step in trying to understand the final secondary structure of PLL in films and the changes, if any, brought about by the addition of the clay is to comprehend the transitions in the secondary structure of PLL in solution state alone. The secondary structure of polypeptides is based on the premise that folding events are driven by the minimum conformational free energy determined by van der Waals interactions, hydrogen bonds, and electrostatic interactions. At high temperatures, the side chain hydrophobic interactions and interchain hydrogen bonds provided by the β-sheet conformation are more stable than the intrachain hydrogen bonds of the α-helix. It is believed that the enthalpy necessary to break the intrachain hydrogen bonds of the α-helix and to associate the hydrophobic side chains is derived from the

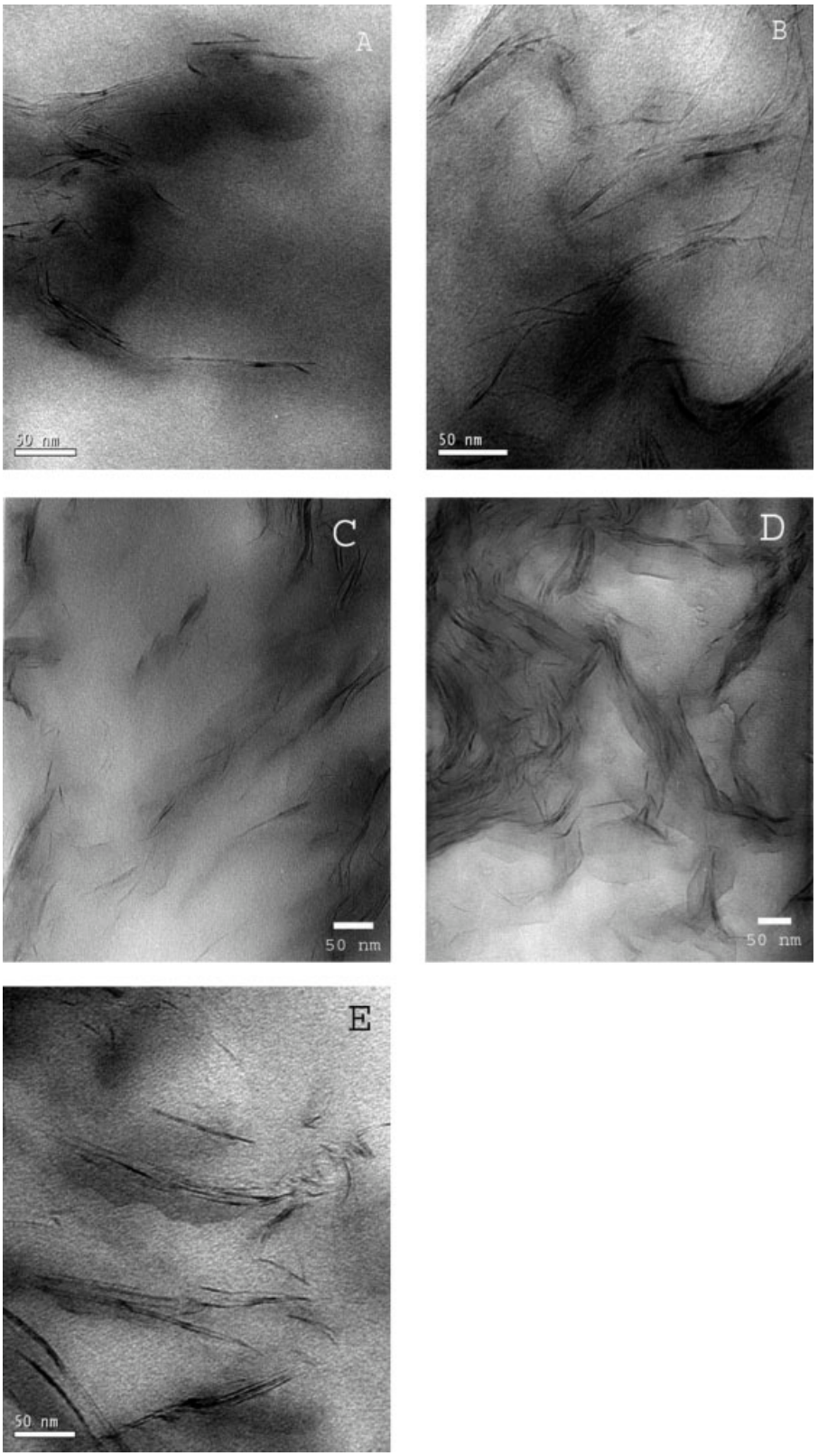

Figure 8. Bright field TEM images of 2 wt % (A), 5 wt % (B), 10 wt % (C), 15 wt % (D), and 2 wt % in low molecular weight (25,500 g/mol) (E) PLL-MMT nanocomposites, showing intercalated regions. Images were obtained on microtomed films (<80 nm) at 200 kV.

heating process. An effect similar to heating the solution is brought about by solution casting into bulk films. During film formation, the evaporation of water brings the α-helical PLL chains close to each other, creating a hydrophobic environment in the interhelical space. The α-helices can interact most favorably while arranged in an antiparallel manner due to their dipole moment.[39] The concentrated, hydrophobic environment in the antiparallel arrangement of the helices can lead to their destabilization and force them into an antiparallel β-sheet structure. Such a transformation of secondary structures is more evident with molecular weights. Dzwolak et al.[39] as well as Jackson et al.[33] have reported on the effect of chain length on the α-helix to β-sheet transition in PLL. Both studies have observed instantaneous conversion of high molecular weight PLL to β-sheet from α-helical solutions. Given the high molecular weight of PLL used, it is therefore not surprising that the secondary structure observed in the films has β-sheet as its major component, even when films are cast from an α-helical PLL solution. Thus, a strong tendency of PLL to transform into a β-sheet structure under certain solution conditions, coupled with its high molecular weight, always produces a β-sheet-rich film.

Results from CD show PLL interaction with clay at low peptide concentrations. Such association can be ascribed to the positive charge of the random coil at low pH (pH 7) and ease of adsorption due to lower entropic penalty of the relatively rigid helix at high pH (pH 11.6). The high aspect ratio clays provide adequate surface area for peptide adsorption, thus facilitating the aforementioned interactions. High peptide as well as clay concentrations during (in solution) and after (in films) nanocomposite formation has been studied using FTIR. A slight increase in the α-helical character with increasing clay loading can be seen in the FTIR data. This can be explained by the interference of the clay platelets with the process of intermolecule aggregation of α-helical chains, decreasing the β-sheet content in the final film. Such interference increases with the amount of clay in the films.

Since it was not possible to control the secondary structure at high molecular weights, it would follow that a greater control over the secondary conformation can be achieved with shorter polypeptide chains/lower molecular weight. This was found in the case of nanocomposite films cast from a relatively lower molecular weight PLL (MW = 25,500 g/mol). These films were richer in their α-helical content (Fig. 5) relative to NCs with higher molecular weight. However, the presence of clay (2 and 5 wt %) at these molecular weights does not change the nature of interactions between PLL and MMT. Experiments[39] have shown that the molecular weight needed for the films to remain α-helical is about 3000 g/mol. We found that contiguous nanocomposite films cannot be obtained with PLL of a molecular weight of 9200 g/mol. Therefore, while providing a contiguous NC film, the highest molecular weight used in this study (84,000 Da/575 residues) leads to films that exhibit a preferred β-sheet secondary structure regardless of the PLL solution conformation present prior to casting.

CONCLUSIONS

Nanocomposites from PLL and MMT clay have been synthesized using the solution casting technique. XRD and TEM reveal intercalated clay nanocomposites; random coil or β-sheet PLL is believed to have intercalated in all samples. The secondary structure of PLL can be controllably altered in solution between random coil, α-helix, and β-sheet using pH and temperature. PLL was found to fold preferentially in the β-sheet structure at the high concentrations relevant to nanocomposite film formation regardless of solution conformation from which films were cast. The transition from α-helix to β-sheet is directly dependant on molecular weight and has a kinetic dependence on temperature. This tendency to form β-sheet in films is stronger with higher molecular weight. Thus, conformational control in terms of α-helix, β-sheet, and random coil nanocomposite films was not possible at high concentrations of the high-molecular-weight polypeptide when casting nanocomposite films from solution. While usage of a very low molecular weight and concentration allows good control of polypeptide secondary structure, these low molecular weights do not lead to the formation of contiguous nanocomposite films. We hope that this insight into the mechanism of secondary structural control in polypeptides will foster the design of new peptidic nanomaterials for specific, desired applications.

Financial support is from NSF Career Award DMR-0348147 and du Pont Young Faculty Award. Beamtime at the National Synchrotron Light Source,

Brookhaven National Laboratory was supported by the U.S. Department of Energy, Office of Science, Office of Basic Energy Sciences (Contract no.: DE-AC02-98CH10886). The authors would like to thank Vahik Krikorian, Yujuan Liu, and Steven Givens for discussions and help.

REFERENCES AND NOTES

1. Giannelis, E. P. Adv Mater 1996, 8, 29–35.
2. Pinnavaia, T. J. Science 1983, 220, 365–371.
3. Alexandre, M.; Dubois, P. Mater Sci Eng R 2000, 28, 1–63.
4. Messersmith, P. B.; Giannelis, E. P. J Polym Sci Part A: Polym Chem 1995, 33, 1047–1057.
5. Gilman, J. W. Appl Clay Sci 1999, 15, 31–49.
6. Brindley, G. W. The X-ray Identification and Crystal Structures of Clay Minerals; Mineralogical Society: London, 1972.
7. Theng, B. K. G. Formation and Properties of Clay-Polymer Complexes; Elsevier: New York, 1979.
8. Ogata, N.; Jimenez, G.; Kawai, H.; Ogihara, T. J Polym Sci Part B: Polym Phys 1997, 35, 389–396.
9. Bjork, N.; Ekstrand, K.; Ruyter, I. E. Biomaterials 1986, 7, 73–75.
10. Jimenez, G.; Ogata, N.; Kawai, H.; Ogihara, T. J Appl Polym Sci 1997, 64, 2211–2220.
11. Kamath, K. R.; Park, K. Adv Drug Delivery Rev 1993, 11, 59–84.
12. Cha, J. N.; Shimizu, K.; Zhou, Y.; Christiansen, S. C.; Chmelka, B. F.; Stucky, G. D.; Morse, D. E. Proc Natl Acad Sci USA 1999, 96, 361–365.
13. Kroeger, N.; Deutzmann, R.; Sumper, M. Science 1999, 286, 1129–1132.
14. Naik, R. R.; Stringer, S. J.; Agarwal, G.; Jones, S. E.; Stone, M. O. Nat Mater 2002, 1, 169–172.
15. Lee, S.-W.; Mao, C.; Flynn, C. E.; Belcher, A. M. Science 2002, 296, 892–895.
16. Shankar, S. S.; Rai, A.; Ankamwar, B.; Singh, A.; Ahmad, A.; Sastry, M. Nat Mater 2004, 3, 482–488.
17. Perry, C. C.; Keeling-Tucker, T. J Biol Inorg Chem 2000, 5, 537–550.
18. Ramakrishna, S.; Mayer, J.; Wintermantel, E.; Leong, K. W. Compos Sci Technol 2001, 61, 1189–1224.
19. Messersmith, P. B.; Giannelis, E. P. Chem Mater 1993, 5, 1064–1066.
20. Zhang, S. Nat Biotechnol 2003, 21, 1171–1178.
21. Krikorian, V.; Kurian, M.; Galvin, M. E.; Nowak, A. P.; Deming, T. J.; Pochan, D. J. J Polym Sci Part B: Polym Phys 2002, 40, 2579–2586.
22. Nazhat, S. N.; Kellomäki, M.; Törmälä, P.; Tanner, K. E.; Bonfield, W. J Biomed Mater Res 2001, 58, 335–343.
23. Nazhat, S. N.; Joseph, R.; Wang, M.; Smith, R.; Tanner, K. E.; Bonfield, W. J Mater Sci: Mater Med 2000, 11, 621–628.
24. Townend, R.; Kumosinski, T. F.; Timasheff, S. N.; Fasman, G. D.; Davidson, B. Biochem Biophys Res Commun 1966, 23, 163–169.
25. Greenfield, N.; Fasman, G. D. Biochemistry 1969, 8, 4108–4116.
26. Davidson, B.; Fasman, G. D. Biochemistry 1967, 6, 1616–1629.
27. Noguchi, H. Biopolymers 1966, 4, 1105–1113.
28. Shibata, A.; Yamamoto, M.; Yamashita, T.; Chiou, J. S.; Kamaya, H.; Ueda, I. Biochemistry 1992, 31, 5728–5733.
29. Greenfield, N.; Davidson, B.; Fasman, G. D. Biochemistry 1967, 6, 1630–1637.
30. Susi, H.; Timasheff, S. N.; Stevens, L. J Biol Chem 1967, 242, 5460–5466.
31. Painter, P. C.; Koenig, J. L. Biopolymers 1976, 15, 229–240.
32. Pederson, D.; Gabriel, D.; Hermans, J. J. Biopolymers 1971, 10, 2133–2145.
33. Jackson, M.; Haris, P. I.; Chapman, D. Biochim Biophys Acta - Protein Struct Mol Enzymol 1989, 998, 75–79.
34. Tomczak, M. M.; Glawe, D. D.; Drummy, L. F.; Lawrence, C. G.; Stone, M. O.; Perry, C. C.; Pochan, D. J.; Deming, T. J.; Naik, R. R. J Am Chem Soc 2005, 127, 12577–12582.
35. Birshtein, T. M.; Zhulina, E. B.; Skvortsov, A. M. Biopolymers 1979, 18, 1171–1186.
36. Zhulina, E. B.; Skvortsov, A. M.; Birshtein, T. M. Mol Biol 1978, 12, 472–479.
37. Padden, F. J., Jr; Keith, H. D.; Giannoni, G. Biopolymers 1969, 7, 793–804.
38. Cui, H. G.; Krikorian, V.; Thompson, J.; Nowak, A. P.; Deming, T. J.; Pochan, D. J. Macromolecules 2005, 38, 7371–7377.
39. Dzwolak, W.; Muraki, T.; Kato, M.; Taniguchi, Y. Biopolymers 2004, 73, 463–469.